

Feasibility Design of Magnetic Auxetic Tactile Sensor for Monitoring the Movement of Human Body

Dongchan Lee

Institute for Advanced Engineering, 175-28, Goan-ro 51 beon-gil, Baegam-myeon, Cheoin-gu, Yongin-si, Gyeonggi-do, 17180, Korea.

Corresponding Author: Dongchan Lee, Institute for Advanced Engineering, 175-28, Goan-ro 51 beon-gil, Baegam-myeon, Cheoin-gu, Yongin-si, Gyeonggi-do, 17180, Korea.

Received date: December 08, 2023; **Accepted date:** December 15, 2023; **Published date:** December 26, 2023

Citation: Dongchan Lee. (2023), Feasibility Design of Magnetic Auxetic Tactile Sensor for Monitoring the Movement of Human Body, *J Clinical Research and Clinical Trials*, 8(4); DOI: [10.31579/2693-4779/174](https://doi.org/10.31579/2693-4779/174)

Copyright: © 2023, Dongchan Lee. This is an open access article distributed under the Creative Commons Attribution License, which permits unrestricted use, distribution, and reproduction in any medium, provided the original work is properly cited.

Abstract

Soft magnetic tactile sensors are versatile devices with potential applications in next-generation flexible electronics. We for the first time developed a new type of soft magnetic tactile sensor called soft auxetic magnetic particle sensor (soft-AMPS) and evaluated its response characteristics. Soft-AMPS contain ferromagnetic powders that are pre-magnetized in a magnetic field, followed by being mixed with a liquid resin, such as polydimethylsiloxane (PDMS) and ECO-FLEX. When an external force is applied to the sensor, the relative distance among the magnetic particles is altered, resulting in a change in the magnetic flux detected by an underlying Hall sensor. The soft-AMPS offers precise sensing with fewer I/O compared to conventional auxetic resistive sensors. Along with its soft materials, the auxetic structure reduces the required force, enhancing wearability. In our research, we compared the Poisson's ratio of the auxetic structure obtained through simulations with that of silicon material. We also compared sensing inputs based on patterns and selected structurally efficient patterns. As a result, our soft-AMPS required approximately 17% of the force to obtain the same amount of input compared to the non-auxetic version and had the sensitivity of 400% to the non-auxetic version. Additionally, the soft-AMPS is calibrated in real-time through a reference Hall sensor, confirming a resolution of 2.9 degrees. The soft-AMPS can be applied to human-robot interaction and human-machine interaction devices by detecting the movement of human body skin in a robot hand/arm or highly sensitive skin sensor.

Keywords: on-skin sensor; magnetic particle sensor; auxetic structure; force sensing

1. Introduction

Recent advancements in wearable technology (Yin et al., 2021), soft robotics (Yasa et al., 2023), human-robot interaction (Kyung and Kim, 2019) (Pang et al., 2020), and human-machine interaction (Dong et al., 2018) have sparked a growing interest in embedded soft devices. Accordingly, various methods have been proposed to manufacture soft sensors that can be integrated into soft systems (Chen et al., 2018) (Zhao et al., 2023).

Soft tactile sensors are manufactured in various sizes, ranging from micrometers (Watatani et al., 2019) to centimeters (Zhu et al., 2021). These are employed in generating device (Shih et al., 2017) (Kim et al., 2022) and robot movements (Roberts et al., 2021)

through shape changes based on flexible structures and precise. Tactile sensors primarily utilize various elements such as resistance (Zheng et al., 2023) (Zhu et al., 2022b), capacitive (Zhu et al., 2022a) (Niu et al., 2022), and optical (Wei et al., 2023) to facilitate the perception of touch. Among these, magnetic-based tactile sensors sense distance, vectors, and other parameters by utilizing an external magnetic field (Man et al., 2022). These magnetic tactile sensors are primarily constructed using materials with skin-like compliance and magnetic powder, and they collect data using 3-Axis Hall sensors (Hellebrekers et al., 2019) (Yan et al., 2021).

To create materials with skin-like compliance, silicone-based elastomers and polyurethane are commonly used (De Boer et al.,

2017). These flexible polymers exist in a liquid state with fluidity before being mixed, forming a mixture with magnetic powder before curing (Nagahama et al., 2019). These mixtures are injected into molds and cured on magnets, or they are fabricated using 3D printing techniques (Hu et al., 2022) (Zhang et al., 2021).

Auxetic structures are characterized by a negative Poisson's ratio, which effectively enhances the sensitivity of sensors based on their mechanical properties (Ren et al., 2018). Sensors incorporating such structures have been studied using various methods, including resistive, piezoresistive, piezoelectric, capacitive, and triboelectric approaches (Kim et al., 2018) (Chang et al., 2023) (Mao et al., 2022) (Dong and Hu, 2023).

In this study, we introduce the hall sensing-based auxetic tactile sensor for the first time. The hall sensing-based auxetic tactile sensor comprises two Hall sensor arrays and a soft auxetic matrix constructed from ferromagnetic powders and eco-flex material. In contrast to previous research, our approach emphasizes not only enhanced sensitivity owing to the Hall sensing mechanism, but also improved wearability and conformality through the adoption of an auxetic structure with a negative Poisson's ratio. To determine an ideal pattern for the auxetic structure, we conducted Finite Element Analysis (FEA) to calculate Poisson's ratios for various patterns, which were empirically validated. We selected a rotating square plate and integrated it with Hall sensing arrays for strain sensing applications. We compared the Poisson's ratio of the auxetic structure obtained through simulations with that of silicon material and sensing inputs based on some patterns, and selected structurally efficient auxetic patterns.

2. Basic Auxetic Structure for Magnetic Auxetic Tactile Sensor

Auxetics are defined as materials or structures with the elastic property of negative Poisson's ratio (NPR): when the material is stretched in one direction, it expands in one or more transverse directions as well. (Ashby and Gibson, 1997) (Gibson et al., 1982) This differs from most materials/structures that typically show a contraction in the perpendicular direction to the stretched direction. Wearable electronic devices can monitor various strains, which is beneficial to human healthcare, medical rehabilitation, soft robotics, human-robot interactions, and human-machine interactions. Strain sensors have received more attention owing to their good conformality, integrability and wearability. To guarantee widespread application, wire strain sensors should possess high sensitivity, high stretchability, and excellent durability. The sensitivity, indicated by the gauge factor (GF), is evaluated by the following equation.

$$GF = \frac{\Delta R/R_0}{\Delta L/L_0} = \frac{\Delta R}{R_0 \varepsilon} = \frac{\Delta C}{C_0 \varepsilon} \approx 1 + 2\nu \quad (1)$$

where $\Delta R / R_0$, $\Delta C / C_0$, R , C , ε and ν denote the relative resistance change, the relative capacitance change, real-time resistance, real-time capacitance, tensile strain, and Poisson's ratio, respectively. When an increasing force (ΔF) applied onto one of the sensing units, the capacitance or resistance is measured for each increment. The

sensitivity S of a capacitance or resistance or magnetic flux can be expressed as,

$$S = \frac{\Delta C/C_0}{\Delta F} = \frac{1}{d_0} \frac{\Delta d}{\Delta F} = \frac{\Delta B}{\Delta F} \quad (2)$$

Where ΔB is the amount of the change in the sensed-magnetic field before and after strain applied, and ΔF is the applied force change. Among the above-mentioned indicators, stretchability and durability are especially important because they ensure large stress loading and stable output of sensing signals after repeated deformation. Although resistance change increases sharply under a large strain, irreversible structural damage appears, and repeated cycling induces a viscoelastic effect, which results in potential fracture and poor durability. To achieve controllable high sensitivity as well as good stretchability and durability, a novel design concept of auxetic materials/structures is integrated with a magnetic field sensing system in this work. The sensitivity of our strain sensors was tuned by tailoring the geometric dimensions of the auxetic structure. Upon mechanical loading, the sensors showed a structural deformation effect (i.e., longitudinal stretching accompanied by transverse structural deformation), which resulted in good stretchability and durability. As the strain increased, continuous stretching produced high sensitivity.

Detailed structural parameters of various auxetic architectures were simulated by a finite element method. The examined auxetic structures are re-entrant hexagon, re-entrant plate, and modified re-entrant hexagon which is composed of re-entrant plate and re-entrant strut in the unit cells. The detailed structural parameters of the auxetic architecture were determined by a finite element modeling simulation. The variable structural Poisson's ratio(ν) was achieved by tailoring the ratio and location of the structural parameters. The produced strain sensors of various patterns exhibited different sensitivities owing to changes in the strain distribution and in the strain levels along the auxetic structural parameters. Based on the FEM simulation, the effective contributions of the patterned strain sensors to the sensitivity were quantified. The structural Poisson's ratio(ν), effective contributions and sensitivity of the auxetic strain sensor were presented to the relationship between the ratio and location of the structural parameters. (Ashby and Gibson, 1997) (Gibson et al., 1982) (Lakes, 2017) The auxetic pattern has negative structural Poisson's ratio(ν) owing to 2D expansion. Its structure geometry includes many parameters, such as thickness, strut angle, width, distance of internal edge, and short straight length on both sides. (Gonella and Ruzzene, 2008) (Masters and Evans, 1996) Among them, thickness and short straight length on both sides were fixed and included angle, width, distance of internal edge were determined by FEM simulation and stress-strain curves. The typical auxetic structures are listed in Table 1. Three architectures were explored as the fundamental pattern. The structural Poisson's ratio(ν) is calculated using eq. (3):

$$\nu = -\frac{\varepsilon_y}{\varepsilon_x} \quad (3)$$

where ε_x and ε_y represent the x-direction strain and y-direction strain.

Table 1: Characteristics of typical auxetic structure

Auxetic Structure	Shape	Poisson's ratios	Young's modulus
<p>Re-entrant hexagon (Ashby and Gibson, 1997) (Gibson et al., 1982) $h = 2l, n = 8$</p>		$v_{12} = -\frac{l \sin^2 \theta}{(h + l \cos \theta) \cos \theta}$ $v_{21} = -\frac{(h + l \cos \theta) \cos \theta}{l \sin^2 \theta}$	$E_1 = n E_s \left(\frac{t}{l}\right)^3 \frac{\sin \theta}{(h/l + \cos \theta) \cos^2 \theta}$ $E_2 = n E_s \left(\frac{t}{l}\right)^3 \frac{(h/l + \cos \theta)}{\sin^3 \theta}$
<p>Modified Re-entrant hexagons (with diamond-shaped cells) (Ashby and Gibson, 1997) (Gibson et al., 1982) $h = 2l, n = 4$</p>		$v_{12} = -\frac{l \sin^2 \theta}{(h + l \cos \theta) \cos \theta}$ $v_{21} = -\frac{(h + l \cos \theta) \cos \theta}{l \sin^2 \theta}$	$E_1 = n E_s \left(\frac{t}{l}\right)^3 \frac{\sin \theta}{(h/l + \cos \theta) \cos^2 \theta}$ $E_2 = n E_s \left(\frac{t}{l}\right)^3 \frac{(h/l + \cos \theta)}{\sin^3 \theta}$
<p>Rotating Triangular Plates (Equilateral) (Grima and Evans, 2006)</p>		$v_{12} = v_{21} = -1$	$E_{1,2} = k_n \frac{4\sqrt{3}}{l^2 \left[1 + \cos\left(\frac{\pi}{3} + \theta\right)\right]}$
<p>Rotating Square Plate (Grima and Evans, 2000)</p>		$v_{12} = v_{21} = -1$	$E_{1,2} = k_n \frac{8}{l^2 [1 - \sin(\theta)]}$

※ Properties of unit cell material: E_s : Young's modulus, ν : Poisson's ratio, k_n : stiffness constant, n : no. of cell strut of re-entrant hexagon, $B=2l \sin \theta$, $H=h+2l \cos \theta$

To estimate the magnetic gauge factor, four auxetic structures with different surface areas can be considered, as shown in Table 2. Poisson's ratio of four auxetic structures is shown in Figure 1 under the loading ranges. On the same locations of magnetic Hall sensors, the influences of the surface magnetic field areas may be verified. Auxetic structures can be integrated into the sensor architecture for improving its sensitivity. Auxetic structures are made to the sensor mixed with the magnetic powder and silicon material. Under application of the principal strain, the negative Poisson's ratio of the auxetic structures causes the width to be increased during sensor deformation, unlike the normal sensors, where the width reduces in a similar situation. In the auxetic sensor, the increased rate of the width

change causes the magnetic flux area expansion and subsequent thickness reduction, therefore affecting the capacitive change, and results in high sensitivity. When stretched, the segments in the auxetic structure rotate, resulting in an extension perpendicular to the direction of the applied strain. This deformation property leads to an increase in the width of the sensor instead of the normal decrease in width. In testing, a strong trend between linearity and the use of auxetic materials may be found, which is ideal for this application due to the increased consistency of the sensor. Additionally, it is found that including the strut's increased consistency at the cost of range of resistance values. Furthermore, it was found that the shaped pattern of re-entrant structure can be found to be the ideal design to optimize linearity of data, in the feasible usability.

Table 2: Characteristics of auxetic structures' geometries

Geometric Type	Re-entrant hexagon	Modified Re-entrant hexagons (with diamond-shaped cells)	Rotating Triangular Plates	Rotating Square Plate

Design Layout (mm×mm)	22×34×1.0	22×34×1.0	22×34×1.0	22×34×1.0
Effective Sensing Surface Area (mm²)	300	354	476	567

Auxetic materials have unusual mechanical properties such as enhanced indentation resistance, vibration damping, and porosity variation that cannot be generally achieved with conventional materials. The auxetic effect of various geometric structures including conventional re-entrant hexagons and modified re-entrant hexagons were examined. Typical cell compositions of each structure are shown in Tables 1 and 2. Finite element analyses (FEA) with tensile & compressive loading conditions were performed on all four geometric structures using the Siemens Simcenter 3D. Tables 1 and 2 show the numerical material properties and geometric dimensions used in TPU (Thermoplastic PolyUrethane).

The trend of Poisson’s ratio was to examine the effect of the tensile force that was varied between -5.0 N and 5.0 N. The bottom surface of

samples in Table 3 was fixed to a rigid structure and various input forces within the given range of forces were applied to the top surface to calculate Poisson’s ratio. All structures show the negative Poisson’s ratios as expected. As higher input forces are applied, the nonlinearity becomes more obvious for different materials. It is close to a linear behavior, but the slight non-linearity is caused by the change of the cell shapes as the auxetic structure is stretched more. To calculate the transverse strain, the displacements in axial and transversal directions are measured along the vertical and horizontal centerlines. Note that the top and bottom surfaces are made of thick solid material to minimize the variation in deformation on both ends. Figures 1 illustrates that Poisson’s ratio is affected by the tensile force for the auxetic structures.

Table 3: Material properties

Material	Density (Kg/m ³)	Young’s Modulus (Pa)	Poisson’s Ratio
TPUs	1200	1.5306×10 ⁷	0.48

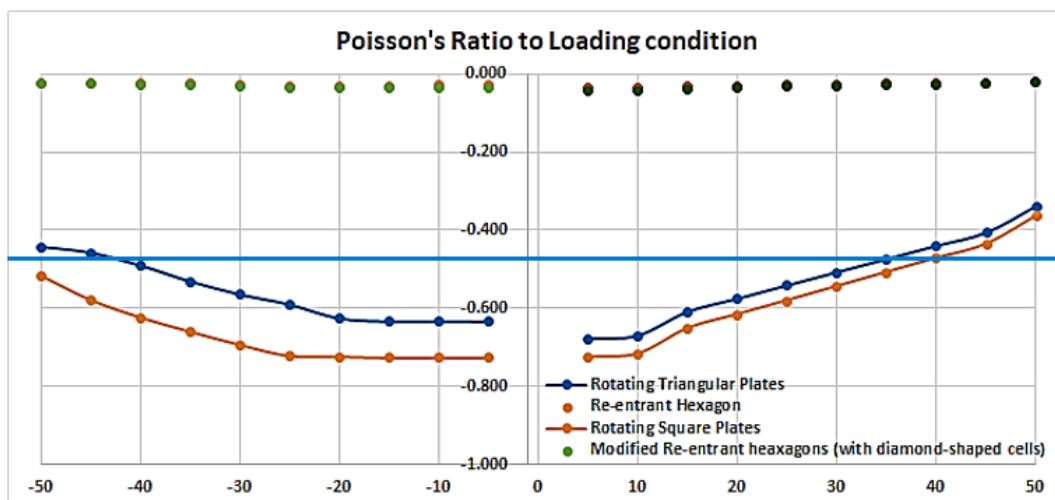


Figure 1: Comparison of Poisson’s ratios obtained from finite element analysis: Re-entrant hexagon, Modified Re-entrant hexagon, Rotating triangular plates and Rotating Square Plates

Notice that Poisson’s ratio for the rotating triangular and square plates have the variable values due to the nonlinearity while the re-entrant hexagons have relatively constant values in the input force range. As Young’s moduli are different for different materials, the Poisson’s ratio is also different for different materials. However, both parameters show the same trend as the input forces are increased because these two pads have the same geometry and dimensions. The ratio of the

strains is mainly the function of cell geometry and the material property in this range of deformation. This magnetic auxetic sensors were applied by various input forces within the given linear range of forces (0~1.0 N) and to the top surface to calculate Poisson’s ratio as shown in Figure 2 and the strain contours of auxetic structure types is shown in Figure 3.

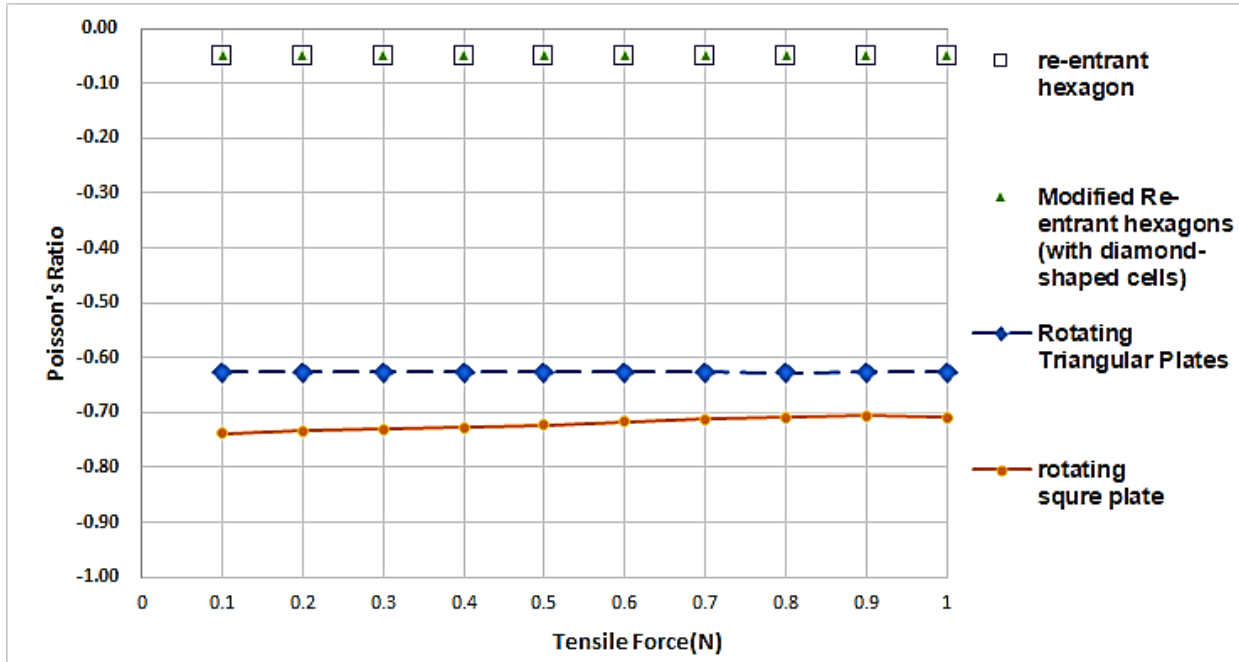
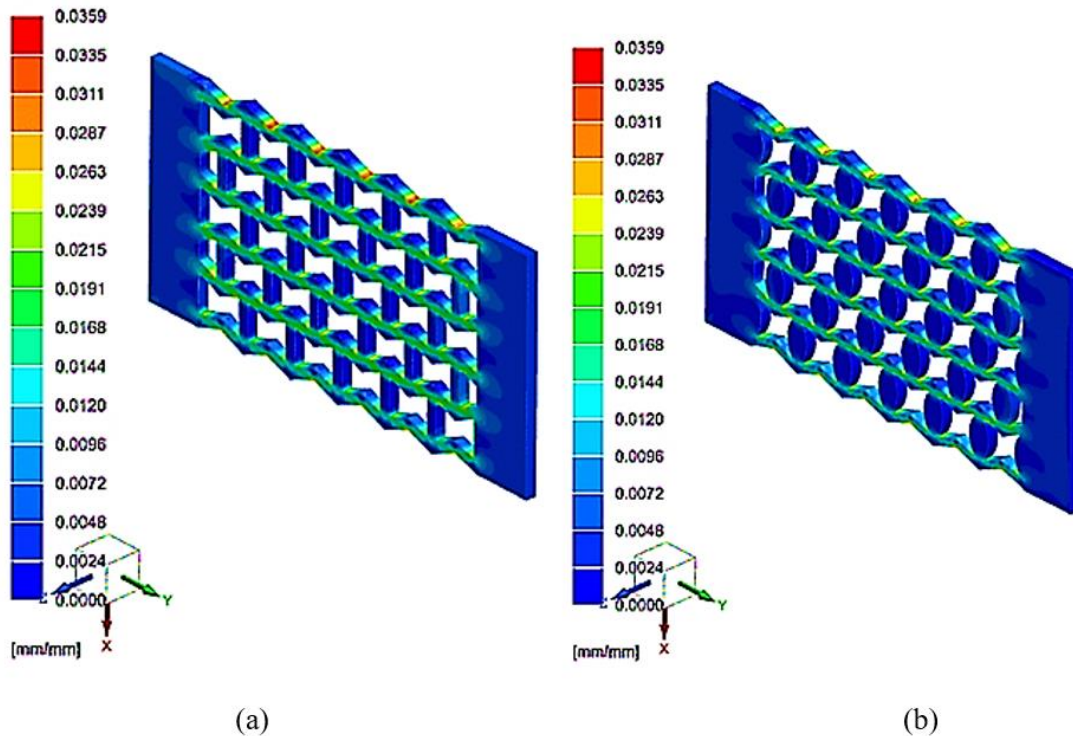


Figure 2: Poisson’s ratio of re-entrant structures for tensile loadings



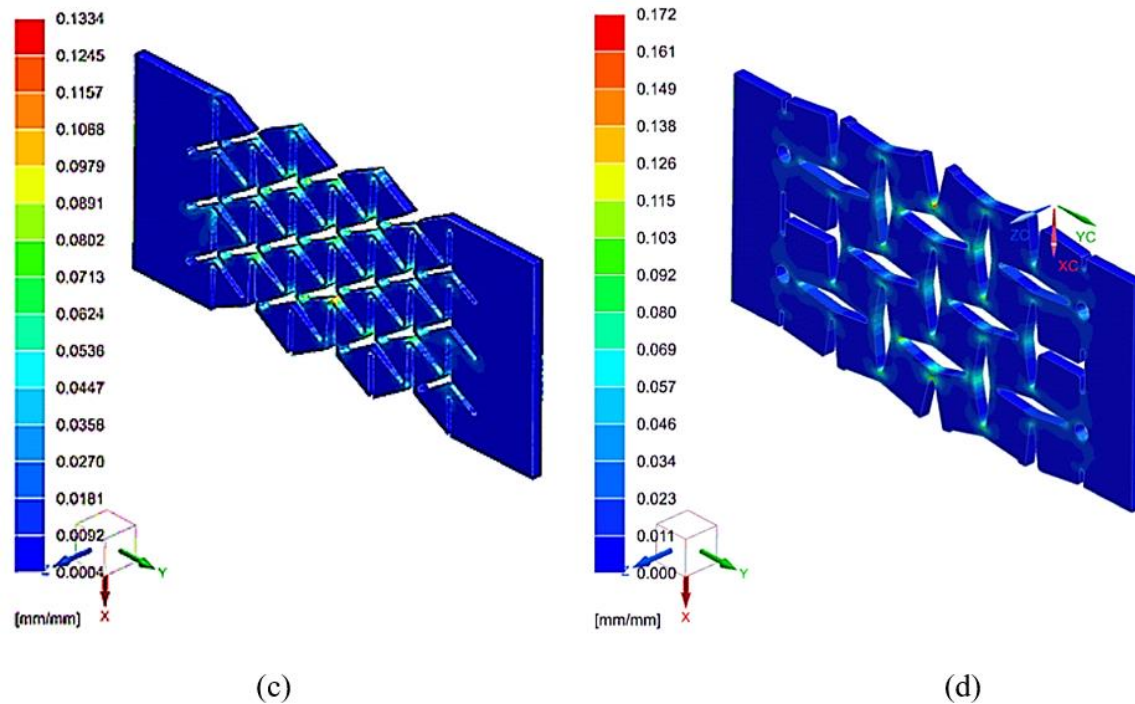


Figure 3: Strain contours of auxetic structure types for tensile loadings; (a) Re-entrant Hexagon, (b) Modified Re-entrant Hexagons (c) Rotating triangular plate, (d) Rotating rectangular plate .

3. Experiments and Results

3.1 Fabrication of Soft-AMPS

The Rotating Square Plate auxetic structure of Soft-AMPS is designed to maintain a rectangular shape, and for this configuration, the material synthesis was carried out to obtain the required properties of silicon material. As shown in Figure 4, Eco-flex (1:1 mixture of casting and hardening materials) and PDMS (10:1 mixture of casting and hardening materials) were mixed at a 1:1 ratio. To prevent curing rejection, it was important to thoroughly mix each solution separately

before combining them. Afterwards, NdFeB particles were added in a 1:1 weight ratio to the mixed silicone solution. In a vacuum chamber, bubbles were removed from the resulting mixture, which was injected into a mold created through 3D printing. To avoid the formation of a pseudo membrane that could reduce the efficacy of the sensor, the solution was carefully injected using a syringe instead of simply pouring and molding it. Next, the mold containing the solution was placed in an oven at 55 degrees Celsius for 3 hours. Once cured, the material was removed from the mold using tweezers.

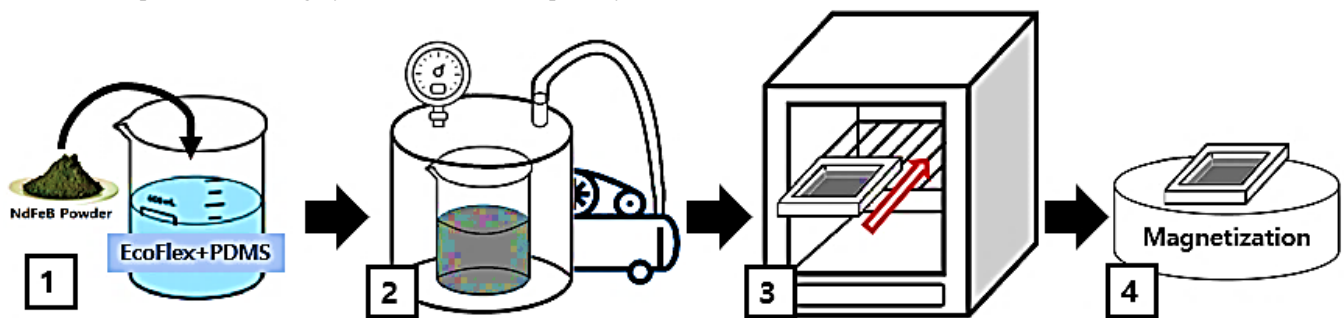


Figure 4: Fabrication process

3.2 Stretchability Test of Auxetic Magneto Tactile Sensor

The fabricated auxetic sensor has been combined with a PCB on which a Hall sensor is mounted as shown in Figure 5 (A) after magnetization on a circular neodymium magnet which has a magnetic field ranging from 300 to 700 mT. To evaluate the characteristics of auxetic structures based on patterns, four samples were prepared as shown in Figure 5 (B). The four samples had dimensions with a thickness of 1.2 mm, a width of 20~22 mm and a length of 33 mm.

They were combined with the circuitry, like the configuration depicted in Figure 5 (A), and securely attached to the top and bottom clamps of a tensile testing machine (ESM303, MARK-10). Magnetic field variations were recorded using a 3-axis Hall sensor (MLX90393). The tensile test was conducted at a speed of 13mm per minute, and magnetic field data was automatically collected during the tensile process. The sum of factors was calculated by adding up the displacements of six data points, which were obtained from the top and bottom 3-axis magnetic vectors. At a 10% tensile strain, the sum of

factors for the re-entrant hexagon was 77uT, for the modified re-entrant hexagon it was 90uT, for the rotating triangular plates it was 99uT, and for the rotating square plates it reached 169uT, as shown in Figure 5 (C). Furthermore, to assess the Poisson's ratio of each sample, the width and length of the samples were measured both before and after the tensile test. The calculated Poisson's ratios were -0.1, -0.12, -0.66, and -0.75, respectively, and this information is visually represented in Figure 5. Overall, the different values were obtained compared to the ones mentioned in section 2, and it was observed that patterns with thinner wires did not experience an increase in width during tension, due to compliant hinge behaviors of auxetic structures. This was attributed to the primary influence of the silicone material on the lack of width expansion.

The main factors that can affect the sum of factors in the magneto tactile sensor are expected to be the uniform distributed quantities of magnetic powders and changes in the magnetic vector. In the auxetic structure, factors that can influence this are seen as numerical values corresponding to the effective sensing region and Poisson's ratio, respectively. The effective surface area is large in the

order of rotating square plate, rotating triangular plates, modified re-entrant hexagon, and re-entrant hexagon, which indicates that the larger surface area, the more amount of magnetic powder. Additionally, the Poisson's ratio is large in the order of rotating square plate, rotating triangular plates, modified re-entrant hexagon, and re-entrant hexagon (1N load or less). As shown in Figure 5 (C), the value of gauge factor is highest on the sample 4 (rotating square plate), which is like to the trend observed in the effective surface area and Poisson's ratio of auxetic structures

When the Rotating Square Plate auxetic structure expands, it induces a change in the angles of each quadrilateral cell. Magnetic powders with a specific magnetic vector undergo rotation along with the quadrilateral cells, resulting in a magnetic field displacement at the position of the Hall sensors. Four Hall sensors are paired up in twos, providing a total of six magnetic vector values as output. These six values are collected as data, with them serving as input and the tensile rate as the output, to be processed through a neural network in deep learning. Soft-AMPS attached to the joint zone are extended and monitored in conjunction with the joint's rotation.

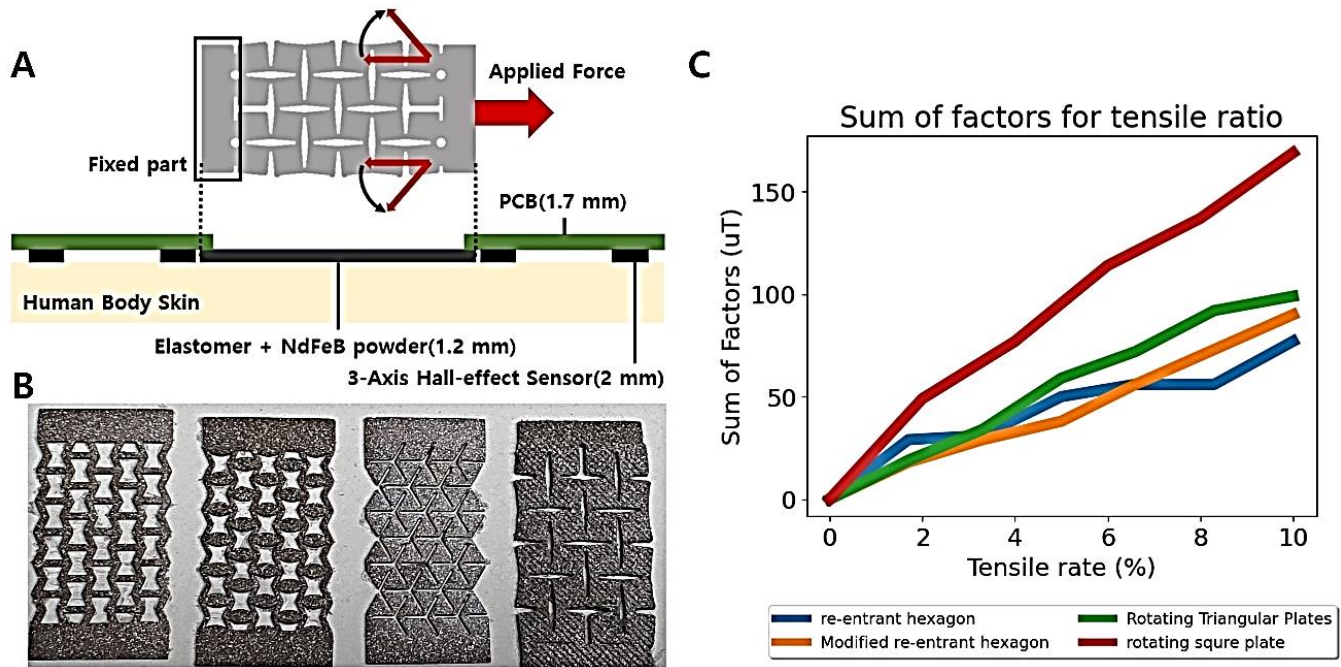


Figure 5: Experiments schematics and results; (A) Illustration of Soft-AMPS, (B) The produced Auxetic samples are in order re-entrant hexagon, modified re-entrant hexagon, Rotating Triangular Plates and Rotating Square Plate, (C) Sum of factors for tensile ratio and Poisson's ratio is -0.1, -0.12, -0.66, -0.75 in that order

3.3 Effects of an Auxetic structure in a Sensor

An auxetic structure requires less force to obtain the same sensing value as a regular rectangular sensor of the same size. Additionally, when stretching the sensor over the same length, an auxetic structure demands less force. In Figure 6 (A), it can be observed that normal samples required approximately force of 1.0 N to induce a displacement of 100uT, whereas the auxetic samples required only about 0.2 N of force to achieve the same displacement. Furthermore, as shown in Figure 6 (B), when subjected to the same amount of tensile

force, it was evident that the auxetic samples required less force compared to the normal samples. This is advantageous for applying sensors to small joints such as finger joints. We prepared a 33mm auxetic sensor and a regular rectangular sensor, both fixed at the length of 5mm of each sensor, in the same configuration. We conducted a tensile test using a testing machine while collecting data through an embedded board, and the experimental setup was identical to Figure 6 (C). The calculated sensitivity using equation (2) shows (110 μT)/(0.2 N)= 550 for the auxetic sensor, and (25 μT)/(0.2 N)= 125 for the conventional sensor.

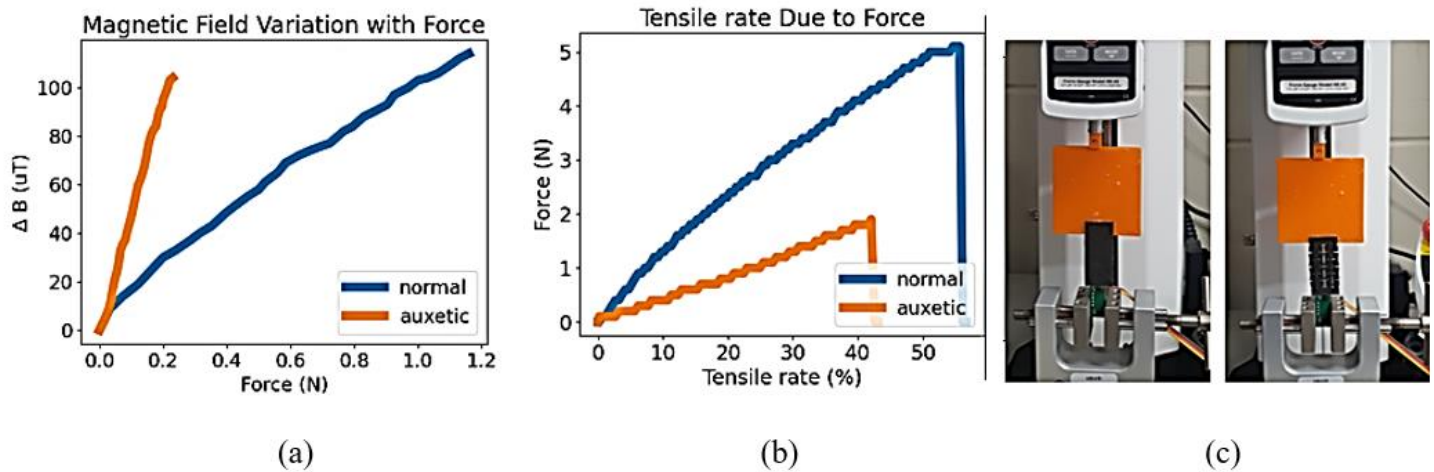


Figure 6: (A) Magnetic Field Variation with Force, (B) Tensile rate Due to Force, and (C) The experimental setup.

4. Discussion and Conclusion

The auxetic pattern-based magneto tactile sensor has the advantage of the properties of the auxetic structure, and the Hall-sensing mechanism: the superior wearability and sensitivity of meta-structures, and the simplicity of the circuitry of Hall-sensing mechanism. In the numerical and experimental aspects, a square rotating pattern showed the highest negative Poisson's ratio among various auxetic patterns. The influence of the mechanical property on the sensor's sensitivity was further studied by integrating the pattern composed of silicone and magnetic particles to the Hall-sensor arrays with the offset calibration function. From the study, we observed a linear increase in the sensitivity with the increase in the Poisson's ratio, indicating a better force localization of the auxetic structure, compared to the non-auxetic pattern.

The newly developed soft-AMPS in this study differs from previous auxetic sensors (Dong and Hu, 2023) in that it utilizes magnetism for sensing. Composed of materials like Ecoflex and PDMS, this material, along with the auxetic structure, is thin and stretchable, designed to be used as a skin strain gauge when attached to the skin. To prevent sensing errors caused by influences like magnetic effects due to movement, real-time offset adjustments were implemented. The auxetic structure and the low I/O magnetic sensor are advantageous for operation on human skin. Compared to non-Auxetic sensors, soft-AMPS has been confirmed to secure a large amount of strain and the required input with minimal force. Through this work, soft-AMPS has been shown to have advantages in features such as strain range, conformability, and wearability. In the future, by employing silicon 3D printing (Vo et al., 2023) to create more complex and efficient structures, it could potentially advance into a higher-performance sensor, becoming a crucial component of on-skin devices.

Acknowledgement

"This research was supported by the Alchemist Project (No. 1415187415, No. 20025750) funded by the Technology Innovation Program funded by the Korea Planning & Evaluation Institute of Industrial Technology (KEIT) and the Ministry of Trade, Industry, & Energy (MOTIE)".

References

1. Ashby, M.F., and Gibson, L.J. (1997). Cellular solids: structure and properties. Press Syndicate of the University of Cambridge, Cambridge, UK, 175-231.
2. Chang, S.-M., Hur, S., Park, J., Lee, D.-G., Shin, J., Kim, H.S., et al. (2023). Optimization of piezoelectric polymer composites and 3D printing parameters for flexible tactile sensors. *Additive Manufacturing* 67, 103470.
3. Chen, W., Khamis, H., Birznieks, I., Lepora, N.F., and Redmond, S.J. (2018). Tactile sensors for friction estimation and incipient slip detection—toward dexterous robotic manipulation: A review. *IEEE Sensors Journal* 18(22), 9049-9064.
4. De Boer, G., Raske, N., Wang, H., Kow, J., Alazmani, A., Ghajari, M., et al. (2017). Design optimisation of a magnetic field based soft tactile sensor. *Sensors* 17(11), 2539.
5. Dong, S., and Hu, H. (2023). Sensors Based on Auxetic Materials and Structures: A Review. *Materials* 16(9), 3603.
6. Dong, W., Wang, Y., Zhou, Y., Bai, Y., Ju, Z., Guo, J., et al. (2018). Soft human-machine interfaces: design, sensing and stimulation. *International Journal of Intelligent Robotics and Applications* 2, 313-338.
7. Gibson, L.J., Ashby, M.F., Schajer, G., and Robertson, C. (1982). The mechanics of two-dimensional cellular materials. *Proceedings of the Royal Society of London. A. Mathematical and Physical Sciences* 382(1782), 25-42.
8. Gonella, S., and Ruzzene, M. (2008). Homogenization and equivalent in-plane properties of two-dimensional periodic lattices. *International Journal of Solids and Structures* 45(10), 2897-2915.
9. Grima, J.N., and Evans, K.E. (2000). Auxetic behavior from rotating squares. *Journal of materials science letters* 19, 1563-1565.
10. Grima, J.N., and Evans, K.E. (2006). Auxetic behavior from rotating triangles. *Journal of materials science* 41(10), 3193-3196.
11. Hellebrekers, T., Chang, N., Chin, K., Ford, M.J., Kroemer, O., and Majidi, C. (2020). Soft magnetic tactile skin for

- continuous force and location estimation using neural networks. *IEEE Robotics and Automation Letters* 5(3), 3892-3898.
12. Hellebrekers, T., Kroemer, O., and Majidi, C. (2019). Soft magnetic skin for continuous deformation sensing. *Advanced Intelligent Systems* 1(4), 1900025.
 13. Hu, H., Zhang, C., Pan, C., Dai, H., Sun, H., Pan, Y., et al. (2022). Wireless flexible magnetic tactile sensor with super-resolution in large-areas. *ACS nano* 16(11), 19271-19280.
 14. Kim, H.W., Kim, T.Y., Park, H.K., You, I., Kwak, J., Kim, J.C., et al. (2018). Hygroscopic auxetic on-skin sensors for easy-to-handle repeated daily use. *ACS applied materials & interfaces* 10(46), 40141-40148.
 15. Kim, M., Yang, J., Kim, D., and Yun, D. (2022). Soft tactile sensor to detect the slip of a Robotic hand. *Measurement* 200, 111615.
 16. Kyung, K.-U., and Kim, S.-Y. (Year). "Soft sensors and actuators for designing new human-robot/machine interaction interfaces", in: 2019 14th ACM/IEEE International Conference on Human-Robot Interaction (HRI): IEEE), 695-695.
 17. Lakes, R.S. (2017). Negative-Poisson's-ratio materials: auxetic solids. *Annual review of materials research* 47, 63-81.
 18. Man, J., Chen, G., and Chen, J. (2022). Recent Progress of Biomimetic Tactile Sensing Technology Based on Magnetic Sensors. *Biosensors* 12(11), 1054.
 19. Mao, L., Pan, T., Ke, Y., Yan, Z., Huang, S., Guo, D., et al. (2022). Configurable direction sensitivity of skin-mounted microfluidic strain sensor with auxetic metamaterial. *Lab on a Chip* 22(8), 1630-1639.
 20. Masters, I., and Evans, K. (1996). Models for the elastic deformation of honeycombs. *Composite structures* 35(4), 403-422.
 21. Nagahama, S., Migita, K., and Sugano, S. (2019). Soft magnetic powdery sensor for tactile sensing. *Sensors* 19(12), 2677.
 22. Niu, H., Chen, Y., Kim, E.-S., Zhou, W., Li, Y., and Kim, N.-Y. (2022). Ultrasensitive capacitive tactile sensor with heterostructured active layers for tiny signal perception. *Chemical Engineering Journal* 450, 138258.
 23. Pang, G., Yang, G., Heng, W., Ye, Z., Huang, X., Yang, H.-Y., et al. (2020). CoboSkin: Soft robot skin with variable stiffness for safer human-robot collaboration. *IEEE Transactions on Industrial Electronics* 68(4), 3303-3314.
 24. Ren, X., Das, R., Tran, P., Ngo, T.D., and Xie, Y.M. (2018). Auxetic metamaterials and structures: a review. *Smart materials and structures* 27(2), 023001.
 25. Roberts, P., Zadan, M., and Majidi, C. (2021). Soft tactile sensing skins for robotics. *Current Robotics Reports* 2, 343-354.
 26. Shih, B., Drotman, D., Christianson, C., Huo, Z., White, R., Christensen, H.I., et al. (Year). "Custom soft robotic gripper sensor skins for haptic object visualization", in: 2017 IEEE/RSJ international conference on intelligent robots and systems (IROS): IEEE), 494-501.
 27. Vo, T.H., Lam, P.K., Sheng, Y.-J., and Tsao, H.-K. (2023). Jammed Microgels in Deep Eutectic Solvents as a Green and Low-Cost Ink for 3D Printing of Reliable Auxetic Strain Sensors. *ACS Applied Materials & Interfaces* 15(27), 33109-33118.
 28. Watatani, K., Terao, K., Shimokawa, F., and Takao, H. (2019). Planar-type MEMS tactile sensor integrating micro-macro detection function of fingertip to evaluate surface touch sensation. *Japanese Journal of Applied Physics* 58(9), 097002.
 29. Wei, R., He, J., Ge, S., Liu, H., Ma, X., Tao, J., et al. (2023). Self-Powered All-Optical Tactile Sensing Platform for User-Interactive Interface. *Advanced Materials Technologies* 8(1), 2200757.
 30. Yan, Y., Hu, Z., Yang, Z., Yuan, W., Song, C., Pan, J., et al. (2021). Soft magnetic skin for super-resolution tactile sensing with force self-decoupling. *Science Robotics* 6(51), eabc8801.
 31. Yasa, O., Toshimitsu, Y., Michelis, M.Y., Jones, L.S., Filippi, M., Buchner, T., et al. (2023). An Overview of Soft Robotics. *Annual Review of Control, Robotics, and Autonomous Systems* 6, 1-29.
 32. Yin, J., Hinchet, R., Shea, H., and Majidi, C. (2021). Wearable soft technologies for haptic sensing and feedback. *Advanced Functional Materials* 31(39), 2007428.
 33. Zhang, X., Hu, H., Tang, D., Zhang, C., Fu, J., and Zhao, P. (2021). Magnetic flexible tactile sensor via direct ink writing. *Sensors and Actuators A: Physical* 327, 112753.
 34. Zhao, Z., Hu, Y.-P., Liu, K.-Y., Yu, W., Li, G.-X., Meng, C.-Z., et al. (2023). Recent Development of Self-Powered Tactile Sensors Based on Ionic Hydrogels. *Gels* 9(3), 257.
 35. Zheng, W., Liu, H., Guo, D., and Yang, W. (Year). "Adaptive Optimal Electrical Resistance Tomography for Large-Area Tactile Sensing", in: 2023 IEEE International Conference on Robotics and Automation (ICRA): IEEE), 10338-10344.
 36. Zhu, J., Zhou, C., and Zhang, M. (2021). Recent progress in flexible tactile sensor systems: From design to application. *Soft Sci* 1(3), 1-14.
 37. Zhu, Y., Chen, X., Chu, K., Wang, X., Hu, Z., and Su, H. (2022a). Carbon black/PDMS based flexible capacitive tactile sensor for multi-directional force sensing. *Sensors* 22(2), 628.
 38. Zhu, Y., Liu, Y., Sun, Y., Zhang, Y., and Ding, G. (2022b). Recent advances in resistive sensor technology for tactile perception: A review. *IEEE Sensors Journal*.



This work is licensed under Creative Commons Attribution 4.0 License

To Submit Your Article Click Here:

Submit Manuscript

DOI:[10.31579/2693-4779/174](https://doi.org/10.31579/2693-4779/174)

Ready to submit your research? Choose Auctores and benefit from:

- fast, convenient online submission
- rigorous peer review by experienced research in your field
- rapid publication on acceptance
- authors retain copyrights
- unique DOI for all articles
- immediate, unrestricted online access

At Auctores, research is always in progress.

Learn more at: <https://auctoresonline.org/journals/clinical-research-and-clinical-trials>